REACTIVITY OF A NiO/Al_2O_3 OXYGEN CARRIER PREPARED BY IMPREGNATION FOR CHEMICAL-LOOPING COMBUSTION

Cristina Dueso[a], Alberto Abad[a], Francisco García-Labiano[a *], Luis F. de Diego[a], Pilar Gayán[a], Juan Adánez[a], Anders Lyngfelt[b]

[a] Department of Energy and Environment, Instituto de Carboquímica (C.S.I.C.)

Miguel Luesma Castán 4, 50018 Zaragoza, Spain

[b] Department of Energy and Environment, Chalmers University of Technology, S-412 96 Göteborg, Sweden

RECEIVED DATE:

Corresponding Author. Tel.: +34-976-733977; fax: +34-976-733318; *E-mail address*: glabiano@icb.csic.es (F. García-Labiano)

Abstract

The reactivity of a Ni-based oxygen carried prepared by hot incipient wetness impregnation (HIWI) on α-Al_2O_3 with a NiO content of 18 wt% was studied in this work. Pulse experiments with the reduction period divided into 4-second pulses were performed in a fluidized bed reactor at 1223 K using CH_4 as fuel. The number of pulses was between 2 and 12. Information about the gaseous product distribution and secondary reactions during the reduction was obtained. In addition to the direct reaction of the combustible gas with the oxygen carrier, CH_4 steam reforming also had a significant role in the process, forming H_2 and CO. This reaction was catalyzed by metallic Ni in the oxygen carrier and H_2 and CO acted as intermediate products of the combustion. No evidence of carbon deposition was found in any case. Redox cycles were also carried out in a thermogravimetric analyzer (TGA) with H_2 as fuel. Both tests showed that there was a relation between the solid conversion reached during the reduction and the relative amount of NiO and $NiAl_2O_4$ in the oxygen carrier. When

solid conversion increased, the NiO content also increased, and consequently $NiAl_2O_4$ decreased. Approximately 20 % of the reduced nickel was oxidized to $NiAl_2O_4$, regardless ΔX_s. $NiAl_2O_4$ was also an active compound for the combustion reaction, but with lower reactivity than NiO. Further, the consequences of these results with respect to the design of a CLC system were investigated. When formation of $NiAl_2O_4$ occurred, the average reactivity in the fuel reactor decreased. Therefore, the presence of both NiO and $NiAl_2O_4$ phases must be considered for the design of a CLC facility.

Keywords: CO_2 capture, chemical-looping combustion, oxygen carrier, nickel oxide, nickel aluminate.

1. Introduction

The continuous increase in the atmospheric concentration of CO_2, mainly coming from the combustion of fossil fuels for power generation, transport and industry, enhances the natural greenhouse effect and contributes to the global warming [1, 2]. Therefore, there is a need to decrease CO_2 emissions in order to stabilize its concentration in the atmosphere. Since fossil fuels are still the dominant energy source worldwide and the transition to renewable energy sources is a slow process, CO_2 capture and sequestration (CCS) has been proposed as an important option to reduce CO_2 emissions from power production. Current CCS technologies, available or under development, have the disadvantage of high costs and energy penalties, associated mainly to the CO_2 capture process, recovering the gas from flue streams [1].

Chemical Looping Combustion (CLC) is a novel combustion technique, proposed initially by Richter and Knoche [3], which combines power production and CO_2 capture in a single stage and produces a pure CO_2 stream ready for compression and sequestration. In a CLC system, the oxygen is transported from the combustion air to the fuel by a solid oxygen carrier (OC) in the form of metallic oxide particles, thus avoiding the dilution of flue gases from the power plant with the N_2 of the air. In this way, the subsequent CO_2 separation is not necessary, with no extra energy need and beneficial exergy efficiencies if CO_2 capture is considered [1, 4-7]. Moreover, 100% CO_2 capture can be virtually reached with CLC process. Another important advantage is the absence of NO_x [8] as a result of the introduction of fuel and air into different reactors and the moderate air reactor operating temperature, about 1400 K.

A common CLC system design [9] consists of two connected fluidized beds, a high-velocity riser for the air reactor (AR) and a low-velocity fluidized bed for the fuel reactor (FR), with the oxygen carrier circulating between them. Fluidized bed reactors

guarantee a good contact between the gas and the solid particles. The gaseous fuel (syngas from coal gasification, natural gas or refinery gas) is oxidized by the oxygen carrier in the FR following the general reaction

$$(2n + m)\, Me_yO_x + C_nH_{2m} \rightarrow (2n + m)\, Me_yO_{x-1} + m\, H_2O + n\, CO_2 \quad (1)$$

where Me_yO_x denotes a metal oxide and Me_yO_{x-1}, its reduced compound. The exit gas stream from the fuel reactor contains mainly CO_2 and H_2O, and almost pure CO_2 is obtained after H_2O condensation.

The reduced oxygen carrier, Me_yO_{x-1}, is transferred to the AR where it is regenerated with air

$$(2n + m)\, Me_yO_{x-1} + (n + m/2)\, O_2 \rightarrow (2n + m)\, Me_yO_x \quad (2)$$

The outlet stream of the air reactor is only composed of N_2 and unreacted O_2. The regenerated oxygen carrier is transported back to the fuel reactor ready for another cycle.

Reaction 2 is strongly exothermic, while Reaction 1 could be either exothermic or endothermic depending on the active metal of the oxygen carrier and the fuel used. The total amount of heat evolved from both reactions is the same as from normal combustion, where the oxygen is in direct contact with the fuel.

The selection of a suitable oxygen carrier is a key issue for the large-scale application of CLC. The oxygen carrier must have sufficient oxygen transport capacity, high reactivity under alternating reducing and oxidizing conditions, high conversion to CO_2 and H_2O, low tendency to carbon deposition, avoidance of agglomeration and high mechanical and chemical stability for successive cycles in a fluidized-bed system. Other requirements are high availability and low cost of the metal, as well as low environmental impact. Several transition state metals, such as Ni, Cu, Mn, Fe and Co have been proposed as the most suitable materials for oxygen carriers in CLC [10-25].

The metallic oxide is usually supported on an inert material, which increases its mechanical strength and provides a higher surface area for the reaction. Oxygen carriers prepared using Al_2O_3, SiO_2, TiO_2 and yttrium stabilized zirconia (YSZ) as binders can be found in the literature.

Ni-based oxygen carriers have shown very high reactivity with methane, main component of natural gas and refinery gas [10, 13, 26-32]. These materials allow to work at high temperatures (1200-1400 K) due to the high melting point of nickel oxide (2228 K) and metallic nickel (1728 K). Nevertheless, thermodynamic restrictions avoid full conversion of the fuel into CO_2 and H_2O and this results in small amounts of CO and H_2 in the outlet gas stream from the FR.

The use of Al_2O_3 as support has been widely studied in the literature [10, 25-31] due to its good fluidization properties and thermal stability. However, a drawback of this material with Ni-based oxygen carriers for its use in CLC is $NiAl_2O_4$ formation [33]. At high calcination temperatures (> 1073 K), part of the NiO can react with the alumina to form nickel aluminate [26], which has lower reactivity than free NiO. Cheng et al. [34] found that free nickel oxide and a surface spinel, $NiAl_2O_4$, are formed when a γ-Al_2O_3 support is impregnated with Ni(II) ions and heated to a temperature about 873 K. The nickel oxide is in weak interaction with the alumina surface and it is easily reducible at temperatures higher than 623 K by H_2, while the nickel surface compound like $NiAl_2O_4$ is in strong interaction with the alumina and it is difficult to reduce below 973 K in H_2 [33].

Although $NiAl_2O_4$ could be reduced by methane, the conversion to CO_2 and H_2O would be lower than for the reaction with NiO. The equilibrium concentrations of CO and H_2 are 9.0 and 13.2 vol. %, respectively, at 1223 K [35]. If the only active phase in the oxygen carrier was $NiAl_2O_4$, it should be not expected that the H_2 and CO

concentrations at the outlet stream were lower than the equilibrium values. In this case, the conversion of gas would be too low and the use of $NiAl_2O_4$ as the only active material in a CLC system would not be acceptable. Cho et al. [36] proposed to use a nickel excess in order to compensate the loss of nickel as nickel aluminate. Other authors have suggested the use of $NiAl_2O_4$ as support instead Al_2O_3 [26-29, 37]. Although its characteristics are suitable for a CLC system, the main drawback is the higher amount of Ni needed. It must be taken into account that nickel is an expensive metal and it can produce environmental problems, so it would be interesting to minimize the active phase content in the oxygen carrier. The addition of Mg and Ca also reduced the interaction of Ni with the support due to the formation of $MgAl_2O_4$ and $CaAl_2O_4$ and improved the stability of the spinel structure in the support material [31, 33-34, 38-41].

Alternatively, Gayán et al. [38] used a thermal treatment of the support, sintering the γ-Al_2O_3 at high temperature to produce its deactivation. In this way, the interaction between the NiO and the support to form the aluminate was minimized. At 1423 K, the phase transformation to α-Al_2O_3 took place. Bolt et al. [42] demonstrated that the interdiffusion of Ni^{2+} and Al^{3+} ions occurs much faster in NiO/γ-Al_2O_3 than in NiO/α-Al_2O_3 samples. Gayán et al. [43] also studied the influence of the preparation method and the nature of the support on the redox properties of NiO/Al_2O_3 oxygen carriers. The oxygen carriers prepared using α-Al_2O_3 showed a weak interaction of NiO with the thermally modified alumina. Independently of the method of preparation, all samples with α-Al_2O_3 showed the presence of free NiO through X-ray diffraction analysis. It is important to maintain a high proportion of this compound to have a high reactivity. Particles prepared by impregnation were selected due to their high reactivity together

with very good fluidization behaviour, low attrition rates and absence of agglomeration problems.

A Ni-based oxygen carrier prepared by hot incipient wet impregnation (HIWI) on α-Al_2O_3 with a NiO content of 18 wt% was used to perform CLC tests in a 500 W_{th} continuous pilot plant for 100 hours using CH_4 (30 vol.%) as fuel [44]. These experiments showed that the relative amount of free NiO in the oxygen carrier varied depending on the oxygen carrier-to-fuel ratio, ϕ, in the CLC process, related to the solid conversion. The relative abundance of free NiO phase decreased when ϕ value decreased and, consequently, the amount of $NiAl_2O_4$ increased. As $NiAl_2O_4$ must be at least partially reduced in a CLC system to fulfil mass balances, temperatures should be high, at least in the range 1123-1173 K, and the oxygen carrier-to fuel ratio higher than 2-3 to obtain high combustion efficiency [44]. No carbon formation was found on particles at these conditions.

The aim of this work is to study the reactivity of a Ni-based oxygen carrier prepared by hot incipient wetness impregnation on α-Al_2O_3 as a function of the content of NiO and $NiAl_2O_4$ in the solid sample. Pulse experiments in a batch fluidized bed reactor and TGA were used to determine the relative amounts of free NiO and $NiAl_2O_4$ as a function of the change in conversion in each redox cycle.

2. Experimental

2.1. Oxygen carrier

A Ni-based oxygen carrier prepared by hot incipient wet impregnation (HIWI) on α-Al_2O_3, designated as Ni18-αAl, has been used in this work. Previous studies showed that high reactivity with Ni-based oxygen carriers using Al_2O_3 as support was achieved when this inert phase was in the form of α-Al_2O_3 [38]. Commercial γ-Al_2O_3 (Puralox NWa-155, Sasol Germany GmbH) particles of 100-300 μm were calcined at 1423 K for 2 h to obtain α-Al_2O_3 (ρ = 1900 kg/m^3, ε = 0.47). The HIWI method [43] involved the addition of a volume of a saturated solution (6 M) of $Ni(NO_3)_2 \cdot 6H_2O$ (> 99.5% Panreac) at 333-353 K over hot α-Al_2O_3 particles (353 K), which corresponded to the total pore volume of the particles. A planetary mixer was used to stir thoroughly the aqueous solution and the solid. Two consecutive impregnation steps were applied to obtain the desired active phase loading (18 wt% of NiO). The resulting solid was calcined at 823 K in air atmosphere for 30 min to decompose the impregnated metal nitrate into the metal oxide. Finally, the oxygen carrier was sintered in a furnace at 1223 K for 1 h.

The experiments of this work were performed with Ni18-αAl particles previously used in a 500 W_{th} continuous pilot plant for 100 hours with CH_4 (30 vol. %) as fuel [44]. The main characteristics of the fresh material and after its use in the CLC continuous pilot plant are shown in Table 1. No major changes in the porosity, density, Brunauer-Emmett-Teller (BET) surface area, mechanical strength or oxygen transport capacity were observed in the particles after its use in the CLC system. The oxygen transport capacity was defined as the mass fraction of oxygen that can be used in the oxygen transfer, calculated as $R_{OC} = (m_{ox} - m_{red})/m_{ox}$. There was not evidence of redistribution or migration of Ni sites during the redox cycles and signs of agglomeration were not observed. The powder XRD patterns of the used Ni18–αAl carrier revealed no new

crystalline phases. Nevertheless, the relative amount of free NiO fell from 65% to 24% of the total Ni in the oxygen carrier after its use in the CLC pilot plant. Consequently, $NiAl_2O_4$ content increased after the operation.

2.2. Fluidized bed reactor

A fluidized bed reactor of quartz was used to determine the gas product distribution and the solid conversion of the Ni18-αAl oxygen carrier. The experimental set-up has been described elsewhere [45]. Different series of 10 reduction-oxidation cycles were carried out using samples of 15 g of oxygen carrier. In each cycle, the reduction period was divided into numerous pulses of 4 seconds in order to investigate smaller conversion intervals. During each pulse, a mixture of 30 vol.% CH_4-70 vol.% N_2 was fed as combustible gas. Between the pulses, N_2 was introduced for one minute to be sure that the remaining gas from the last pulse had left the reactor system. In order to avoid a large increase in the reactor temperature during the oxidation step, a gas mixture with 5 vol.% O_2 in N_2 was used instead pure air, with an oxidation time of 500 s. To avoid mixing of CH_4 and O_2, nitrogen was introduced for 3 min after each reducing and oxidizing period. Depending on the number of pulses, a different conversion of the oxygen carrier was achieved at the end of the reduction period. This method allowed to study the relation between the degree of conversion and the reactivity of the solid. After the 10 redox cycles of each test, a reference cycle with 5 pulses of 4 s during the reduction using 50 vol.% CH_4 was conducted in the fluidized bed reactor. This reference cycle was used to compare oxygen carrier reactivity and gas product distribution obtained depending on the variation of solid conversion during the redox cycles.

All tests were carried out at 1223 K with an inlet gas flow of 900 mL_N/min (NTP: normal temperature and pressure) for the reacting gas. For the inert and the oxidizing period, the gas flows were 900 and 1000 mL_N/min, respectively.

The solid conversion was calculated from the outlet concentrations of CO_2, CO and H_2O by means of the following equation

$$X_s = \frac{2n_{CO_2} + n_{CO} + n_{H_2O}}{n_O} \quad (3)$$

where n_i is the number of moles of the gas i measured during the whole reduction time of a redox cycle and n_O is the total number of oxygen moles available for the reduction reaction in the oxygen carrier. H_2 and H_2O concentrations could not be measured but they were calculated from mass balances and considering that the outlet gas concentrations were those from the water gas shift equilibrium (WGS) at the operating temperature [45]

$$CO + H_2O \leftrightarrow CO_2 + H_2 \quad (4)$$

2.3. Reactivity tests in TGA

Reactivity tests of Ni18-αAl oxygen carrier were carried out in a thermogravimetric analyzer (TGA), CI Electronics type, at 1223 K. Detailed information about this experimental facility was described elsewhere [10]. The oxygen carrier was loaded in a platinum basket and heated to the set operating temperature in air atmosphere. After weight stabilization, the experiment was started by exposing the oxygen carrier to alternating reducing and oxidizing conditions. Reactivity data as a function of time were obtained from the weight variations during the reduction-oxidation cycles. The reacting gas was composed by 5 vol.% H_2 and N_2 (balance) and the gas used for oxidation was

100 vol.% air. Nitrogen was introduced for 2 min after each reducing and oxidizing period to avoid mixing of combustible gas and air.

To convert data into solid conversions the involved chemical reactions (Reactions 1 and 2) were considered. The solid conversion was calculated by means of the following equation

$$X_s = \frac{m_{ox} - m}{m_{ox} - m_{red}} \quad (5)$$

where m is the actual mass of sample, m_{ox} is the mass of the sample when it is fully oxidized, and m_{red} is the mass of the sample in the fully reduced form.

Six experiments with 10 redox cycles using different reaction times (Table 2) were carried out in the TGA to achieve, consequently, different solid conversions in each of them. The oxidation time, 180 s in all cases, was also included in Table 2. Previous experiments had demonstrated that $NiAl_2O_4$ formation was not affected by the length of the oxidation period, so the oxidation time was selected only to assure complete oxidation of the oxygen carrier. After the 10 redox cycles, two different tests were carried out to analyze the relation between the degree of conversion and the fraction of NiO and $NiAl_2O_4$ present in the oxygen carrier. The first one consisted of a long cycle with complete conversion of the oxygen carrier. In the second series, a temperature-programmed reduction (TPR) analysis of the sample was performed in the same TGA system with 15 vol.% H_2 and heating the sample to 1223 K at 20 K/min. In the TPR experiments it was possible to separate the reduction of free NiO from that of $NiAl_2O_4$ and thus to determine the fractional amount of each one.

3. RESULTS AND DISCUSSION

3.1. Pulse experiments in batch fluidized reactor

Several experiments were carried out in a batch fluidized bed reactor to study the reactivity of the Ni18-αAl oxygen carrier and to analyze the product distribution during the reduction period. To analyze the conversion intervals more accurately, the reduction time was divided into pulses of 4 seconds, with 1 minute of inert gas between them.

3.1.1. Distribution of gaseous products

Figure 1 shows an example of the product distribution during a reduction period consisting of 12 pulses of CH_4. It has to be highlighted that the concentrations are quite low because the methane was diluted with the nitrogen flow introduced between the pulses. As can be seen, most of the CH_4 was converted to CO_2 in the first pulse. During the first three pulses, CO_2 concentration remained almost constant and, so, CO concentration did not vary either, with very low values. As the oxygen carrier was more reduced and the amount of available oxygen was diminishing, CO_2 concentration decreased and CO increased with each pulse. CH_4 left the reactor only during the first pulse in a very low concentration and disappeared in the second pulse, achieving a fuel conversion almost complete during the whole reaction time.

By means of the analysis of the distribution of gaseous products, we can obtain important information about secondary reactions during the oxygen carrier reduction with CH_4, e.g. methane steam reforming and carbon formation through methane decomposition or Boudouard reaction. Johansson et al. [45] attributed the small amount of unreacted CH_4 during the first pulse to the lack of Ni^0 sites on the fully oxidized particles. When the reduction reaction progressed and the content of Ni increased, CH_4 disappeared. In this case, most of the unconverted gases were CO and H_2. This suggested that the steam reforming of CH_4, catalyzed by metallic nickel, was a reaction that contributed to the conversion of CH_4 [26]

$$CH_4 + H_2O \leftrightarrow CO + 3\,H_2 \quad (6)$$

CO and H_2 act as intermediate products during CH_4 reaction with the Ni18-αAl oxygen carrier. This reaction mechanism of the combustion through the steam reforming reaction could explain the absence of CH_4 in the outlet gases, even when CO concentrations were quite high.

3.1.2. Carbon formation

Pulse experiments were also used to study carbon formation during CH_4 combustion with the Ni18-αAl oxygen carrier. A suitable oxygen carrier for chemical-looping combustion process should not promote the formation of carbon during the oxidation of the fuel. Carbon deposition could have negative effects on the particles, such as deactivation of the oxygen carrier and/or agglomeration problems in the system. Depending on the operating conditions, carbon can be gasified with the CO_2 and H_2O present in the FR or it could be transferred with the solid particles to the AR, where it would be burnt with the oxygen of the fed air. The release of CO and/or CO_2 in the AR together with the N_2 and the unused O_2 would cause a decrease in the CO_2 capture efficiency of the CLC process.

Carbon formation in the fuel reactor mainly takes place through two ways: methane decomposition (7) and Boudouard reaction (8).

$$CH_4 \rightarrow C + 2\,H_2 \quad (7)$$

$$2\,CO \rightarrow C + CO_2 \quad (8)$$

Both reactions are slow in the absence of a catalyst, but metallic Ni formed during the reaction of the oxygen carrier with the fuel can catalyze them.

The carbon deposition can be determined by the analysis of the curves of CO and CO_2 concentration during consecutive pulses. Figure 2 shows the concentration of CO and

CO_2 from pulses 1, 4, 6, 8 and 10, corresponding to a redox cycle with 10 pulses of 4 s during the reducing period. These profiles are close to the pattern of a Gaussian curve due to the dispersion of the gases in the transport lines of the system. A slight tail in the Gaussian curve was detected in the latter part of the curve for every pulse because the dispersion in the pipes was high [46]. A different profile was observed by Johansson et al. [45] when carbon formation happened. The carbon formation was proved by a significant shoulder of either CO_2 and/or CO leaving the reactor during the inert period between pulses. The presence of CO or CO_2 during the inert period was due to a solid-solid reaction with the remaining oxygen in the particles.

$$C + Me_yO_x \rightarrow CO + Me_yO_{x-1} \rightarrow CO_2 + Me_yO_{x-2} \quad (9)$$

However, the characteristic shoulder in concentration profiles due to the reaction of carbon with NiO was not observed. Moreover, neither CO nor CO_2 were measured during the oxidation period. This fact indicates that there was no carbon formation during the reduction stage.

Previous work using the same nickel-based oxygen carrier had shown no tendency to carbon deposition [43-44, 47-49]. When Ni18-αAl was used in a 500 W_{th} CLC continuous pilot plant, neither CO or CO_2 were detected in the air reactor, indicating that there was no carbon deposition in the fuel reactor, independently of the selected fuel (CH_4 or syngas), the presence of impurities in the fuel gas, such as sulphur or light hydrocarbons, or the operating conditions (fuel reactor temperature, solids circulation rate). The high reactivity of the oxygen carrier particles could explain the absence of carbon formation. Carbon can also be gasified quickly to form CO and H_2 that are subsequently oxidized by the oxygen carrier, avoiding its detection. Cho et al. [36] suggested that carbon formed during the period when the fuel conversion was high,

1 could be a possible reaction intermediate and that methane conversion proceeded via
2 carbon and hydrogen oxidation on the surface of the oxygen carrier.
3 Successive reduction-oxidation cycles performed in a batch fluidized reactor in a
4 previous work [43] showed that, initially, when CH_4 was fed to the system, the
5 conversion was complete and mainly selective to CO_2 and H_2O for more than 70
6 seconds. When the solid conversion was about 25 %, CO and H_2 concentrations started
7 to increase while CO_2 and H_2O concentrations decreased. The formation of carbon took
8 place in this period, when less oxygen was available in the reactor, and it was detected
9 by the presence of CO and CO_2 during the oxidation stage. Nevertheless, formed carbon
10 could affect the obtained results with respect to reactivity of the Ni-based oxygen carrier
11 taking into account the work of Cho et al. [36]. In the pulse experiments carbon
12 deposition was not observed, as in the experiments in the pilot plant, so the obtained
13 information about reactivity was closer to that kind of continuous systems.
14

15 **3.1.3. Analysis of the oxygen carrier reactivity**

16 To analyze the reactivity of the Ni18-αAl oxygen carrier during successive redox
17 cycles, normalized concentrations of CO and CO_2 were calculated as the ratio between
18 the CO or CO_2 partial pressure and the sum of partial pressures of the carbon-containing
19 gases in the outlet stream of the batch fluidized bed reactor.

20 $$\gamma_{CO} = \frac{P_{CO,out}}{P_{CH_4,out} + P_{CO_2,out} + P_{CO,out}} \quad (10)$$

21 $$\gamma_{CO_2} = \frac{P_{CO_2,out}}{P_{CH_4,out} + P_{CO_2,out} + P_{CO,out}} \quad (11)$$

22 where $P_{i,out}$ is the partial pressure of outgoing gaseous species i in dry basis.
23 Figures 3a and 3b show CO and CO_2 normalized concentrations in the outlet gases of
24 the reactor as a function of the solid conversion, corresponding to experiments with 4

and 10 pulses during the reduction period, respectively. In both cases, it can be distinguished a first section of the reduction where the CO_2 concentration remained above 90% followed by a sharp decrease and, therefore, an increase of CO concentration. The value of solid conversion where this change was observed depended on the number of cycle and the number of pulses in each redox cycle.

On the one hand, differences were observed in the CO and CO_2 concentrations with respect to the number of cycle. As seen in Figure 3, the outlet concentrations of CO and CO_2 became stable from the second cycle when the reduction period consisted of 4 pulses of CH_4. Nevertheless, when the reduction stage was divided into 10 pulses, five cycles were necessary to achieve a stable value of concentration of the carbon-containing gases, with the differences between the cycles being more distinct in this case. On the other hand, the evolution of CO and CO_2 concentration with the solid conversion changed significantly depending on the total number of pulses in each cycle. Thus, to observe a considerable increase in CO concentration, it was necessary to reach a solid conversion about 0.2 and 0.4 for the 4 and 10-pulse cycles, respectively, after stabilization. This clearly indicated a significant difference in the reactivity of the Ni18-αAl oxygen carrier depending on the number of the cycle and the number of pulses. The faster the CO_2 concentration started to decrease and CO to increase, the less reactive the oxygen carrier was.

The evolution of the oxygen carrier reactivity with the number of pulses and cycles can be inferred from data shown in Figure 4. The solid conversion needed to reach a normalized CO_2 concentration of 90% in every cycle for experiments with 2 to 12 pulses of methane during the reduction of the fuel is shown in this Figure. There are three different tendencies in the curves depending of the number of CH_4 pulses. When 2 pulses were used, the curve had a negative slope, indicating that the reactivity of the

oxygen carrier decreased with the number of cycles. For tests with 4 and 6 pulses, the solid conversion hardly varied during the whole series of 10 cycles. Nevertheless, with a higher number of pulses, the solid conversion increased with the number of cycles, indicating an increasing reactivity of the oxygen carrier.

To analyze better the reactivity of Ni18-αAl oxygen carrier with different number of pulses in the reduction, a reference cycle with the same conditions in all cases (5 pulses, 50 vol. % CH_4) was performed after the series of 10 redox cycles. Figure 5 shows the solid conversion obtained in this reference cycle for particles having different number of pulses and the original oxygen carrier recovered from the continuous CLC pilot plant. As can be seen, there was an initial period of high reactivity where the curves were overlapped. Then, there was a change of slope in the curves of conversion in all cases, which corresponded to a decrease in reactivity. This change of reactivity occurred at different solids conversion depending of the number of pulses in the reduction. The inflection point shifted to higher values with the number of pulses. The observed tendency is the same as the one described for Figure 4. Low number of pulses meant that the inflection point shifted to lower values of solids conversion than the one obtained with the initial sample in the reference cycle. If the number of reduction pulses increased, the solids conversion at the inflection point was higher than the one reached with the initial sample.

Changes in reactivity observed in these tests are related to different relative amounts of free NiO and $NiAl_2O_4$ in the oxygen carrier, as will be shown below. The first period of high reactivity is attributed to the fast reaction of the free NiO with CH_4, and the second period of lower reactivity corresponds to the reduction of $NiAl_2O_4$ [44]. The formation of $NiAl_2O_4$ affects negatively to the methane combustion selectivity towards CO_2 and H_2O since the rate of oxygen release by $NiAl_2O_4$ is lower than the one of NiO. In

previous works, during experiments carried out in a 500 W_{th} continuous pilot plant [44], it was observed that the relative abundance of free NiO decreased when there was a decrease in the change of the solids conversion that occurred in the cycle from air to fuel reactor and back, i.e. when circulation was increased. Reactivity of the NiO phase is different from that of the $NiAl_2O_4$ phase, which explains the change in reactivity of the oxygen carrier with the variation of solid conversion.

During the pulse experiments, when the number of pulses increased, the solid conversion reached during the test also increased, and so the reactivity. The amount of free NiO can be estimated from the point where the curve of conversion changed the slope, i.e. the amount of free NiO was related to the first period of high reactivity. Figure 6 shows the amount of free NiO in the samples as a function of the solid conversion reached after the last reduction cycle for different number of pulses. As can be seen, the relative amount of free NiO was lower than the solid conversion in the reduction period. This means that a fraction of the reduced Ni was converted into $NiAl_2O_4$ during the oxidation. It was estimated from the shading area in the graph, which includes all obtained data, that about 60-85% of the reduced Ni was oxidized to nickel oxide, and, consequently, 15-40 % of Ni was oxidized towards $NiAl_2O_4$. This reaction of metallic nickel to $NiAl_2O_4$ seems to be a too complex reaction to take place in only one step. The fraction of $NiAl_2O_4$ in the oxygen carrier depended on the solid conversion during the reduction, i.e. the amount of metallic Ni formed and subsequently that needed to be oxidized. Therefore, Ni was not unequivocally joined to a molecule of Al_2O_3 to form $NiAl_2O_4$. From this, it can be suggested that the formation of $NiAl_2O_4$ took place through two steps. Firstly, metallic Ni was oxidized to NiO and then, part of this NiO reacted with the alumina to form $NiAl_2O_4$ while the rest remained as free NiO in the oxygen carrier.

In Figure 6, the fraction of NiO as a function of the solid conversion for the original Ni18-αAl particles is also shown (see black point). These particles were previously used in a 500 W_{th} continuous CLC unit with a variation of the solid conversion about 32% and a NiO content about 24%. The conversion data of the original sample was very close to the ones obtained in the tests with 4 and 6 pulses, about 25-35%. When the reduction period was composed by 2 pulses, the solids conversion was 14%, lower than the 32% reached in the CLC system for the original sample. Correspondingly, the fraction of NiO in the oxygen carrier decreased and the reactivity and the NiO content were also lower (Figures 4 and 5). Nevertheless, when the number of pulses during the reduction was higher than 6, the solids conversion was higher than 50%. In these cases, the opposite effect was observed, i.e. NiO content increased as well as reactivity. In conclusion, if there was no variation in the solid conversion with respect to the initial sample, the amount of NiO would remain constant through the cycles as indicated by the straight lines shown in Figure 4. However, if the solid conversion during the reduction period was varied, the content of NiO would stabilize in a new value, which would be higher or lower than the initial one when the solid conversion increased or decreased, respectively. This fact is clearly visible in Figure 4.

3.2. Thermogravimetric experiments

The pulse experiments carried out in the batch fluidized bed reactor gave interesting information about CH_4 conversion, secondary reactions and NiO/$NiAl_2O_4$ distribution in the Ni18-αAl oxygen carrier. Nevertheless, they provided only a few conversion-time data in each cycle so it was difficult to determine accurately the solid conversion where the change of reactivity from NiO to $NiAl_2O_4$ took place, obtaining a great dispersion in

the NiO fraction present in the oxygen carrier (60-85%). For this reason, additional tests were performed in a thermogravimetric analyzer.

The experimental series in TGA consisted of 10-redox-cycle experiments. In each experiment, different reduction times were used to achieve different solid conversions. These tests were carried out twice. At the end of the first series, a redox cycle long enough to reach complete conversion during the reduction was done. After the second series, the samples were cooled and a temperature programmed reduction (TPR) analysis was performed to analyze the relative amount of NiO and $NiAl_2O_4$ in the oxygen carrier. In all TGA tests, 5 vol.% H_2 was used as fuel and the temperature was 1223 K.

In a similar way to the pulse experiments, the conversion-time curves varied during the first redox cycles until they were stabilized. Figure 7 shows the conversion-time curves for the reference cycle after 10 redox cycles with different times of reaction as was indicated in Table 2. The reduction of the oxygen carrier particles proceeded in two stages. In the first seconds, the reaction was fast and all the samples followed the same trend with curves almost overlapped. Then, there was a slope change in the curves due to a decrease in reactivity. The conversion value in which the slope of the curves changed was a function of the reduction time during the 10 previous redox cycles. As can be seen in Table 2, when the reduction time increased, the solid conversion reached also increased. A relation between the variation of solid conversion during the redox cycle and the reactivity of the oxygen carrier was proved, agreeing with the results obtained from the pulse experiments.

H_2-TPR analysis of the solids allowed determination of the relative amount of NiO and $NiAl_2O_4$ in the oxygen carrier. Figure 8a shows TPR of the samples after the TGA experiments from Table 2. Each curve shows two peaks of H_2 consumption which

corresponded to literature data [33, 50-52]. Several works about Ni/Al_2O_3 catalysts reported a H_2 consumption peak in the low-temperature range of 650-900 K and a high-temperature peak with a maximum near 1150-1200 K. The peak in the low-temperature range is attributed to the reduction of Ni^{2+} in the free NiO phase, whereas the high-temperature one corresponds to the reduction of Ni^{2+} in the $NiAl_2O_4$ spinel. It can be observed in Figure 8 that the peak corresponding to NiO reduction increased when the time of the reduction period increased, i.e. the solid conversion increased. The opposite effect was registered for $NiAl_2O_4$ peak.

Figure 8b also shows the solid conversion of samples during TPR carried out in TGA. The first increase in the solid conversion corresponds to the H_2-consumption peak of NiO reaction and the second one to $NiAl_2O_4$ reduction. Thus, NiO amount in the oxygen carrier can be obtained from the conversion corresponding to the flat part of the curve. NiO fraction was depicted in Figure 9 as a function of the conversion reached in the TGA experiments. As the variation of solid conversion increased, the relative amount of NiO also increased and, therefore, the fraction of $NiAl_2O_4$ decreased. However, the relative fraction of NiO after oxidation was lower than the conversion of the oxygen carrier during the reduction period. According to Figure 9, about 80% of the reduced Ni was oxidized to NiO and remaining Ni was oxidized to $NiAl_2O_4$. These results agree with the ones found in the previous batch fluidized bed reactor tests and experiments in a 500 W_{th} continuous CLC pilot plant [44].

The influence of the oxidation degree on the $NiO/NiAl_2O_4$ ratio was also studied by means of a new experiment in the TGA with the oxygen carrier partially oxidized (≈ 50% oxidized). A fraction of metallic Ni remained in the particles during the cyclic test, in a similar way as in a real scale CLC pilot plant, where the solid is not fully oxidized.

As it was found previously, about 80% of the metallic nickel formed during the reduction step was oxidized to NiO while the rest reacted to $NiAl_2O_4$.

4. Application to a CLC system design

The more relevant parameters to take into account in the design of a CLC system are the solid inventory in the FR and the AR, and the solids circulation rate between both reactors. The solid circulation rate must be high enough to transfer the oxygen necessary for the fuel combustion and to supply the heat to maintain the heat balance, especially when CH_4 is used as fuel with Ni-based oxygen carriers, because the reduction reaction is endothermic. Abad et al. [11] defined the solids circulation rate, $\dot{m}_{OC}$, expressed as mass flow of fully oxidized oxygen carrier, through Equation 12

$$\dot{m}_{OC} = \frac{2dM_O}{R_{OC}\Delta H_c^{\,o}} \frac{\Delta X_g}{\Delta X_s} \tag{12}$$

The solid inventories can be determined from a mass balance of solids and gases in both reactors of the CLC system. Assuming perfect mixing of the solids and gas plug flow, with no resistance to the gas exchange between bubble and emulsion phases in the fluidized bed, the solids inventory in the FR per MW of fuel, m_{OC}, will be given by [11]

$$m_{OC} = \frac{2dM_O \Delta X_g}{R_{OC}\Delta H_c^{\,o}} \left[\overline{\frac{dX_s}{dt}}\right]^{-1} \tag{13}$$

$\left[\overline{\frac{dX_s}{dt}}\right]$ represents the average reactivity of the oxygen carrier in the fuel reactor. It is desirable to minimize the amount of material in the system because this will reduce the size and investment cost necessary, but this must be enough to supply the required amount of oxygen for the total conversion of the fuel. So a highly reactive oxygen carrier would be suitable for CLC.

The results shown in this work will have important consequences for the CLC design as will be explained below. Thermodynamic calculations show that $NiAl_2O_4$ has low selectivity towards CO_2 and H_2O, with CO and H_2 concentrations in the equilibrium of 9.0 and 13.2%, respectively, against 0.32 and 0.44% when CH_4 reacts with NiO.[35] Despite its low reactivity, the results obtained in TGA, batch fluidized bed reactor and continuous pilot plant indicates that $NiAl_2O_4$ must also react to fulfil mass balances. Indeed, if a fraction of reduced Ni is oxidized to $NiAl_2O_4$ in the air reactor, this fraction should be reduced again to Ni in the fuel reactor. Nevertheless, the need of $NiAl_2O_4$ reduction does not mean that fuel conversion is reduced, as was proven in a previous work [44] where Ni18-αAl oxygen carrier was used in a continuous unit. The reason for this is the presence of the highly reactive NiO compound. Here it is necessary to point out that, in a fuel reactor, where it can be assumed that there is perfect mixing for solids, NiO is not exhausted before $NiAl_2O_4$ is reduced, but NiO and $NiAl_2O_4$ are being reduced at the same time and some of the unreacted NiO remains always in the FR. Thus, the presence of NiO permits a high conversion of the fuel gas into CO_2 and H_2O. Taking into account the above considerations, all Ni present in the oxygen carrier was considered active for the oxygen transference. The oxygen transport capacity was the corresponding to 18% Ni, which has relevance on the solid circulation rate between the fuel and air reactor as it was indicated by Equation 12. The minimum solids circulation rate for Ni18-αAl, calculated when $\Delta X_s = 1$, is 2 kg OC s^{-1} MW_f^{-1}.

Calculations of reactivity with NiO/$NiAl_2O_4$ oxygen carriers are usually made considering that all reactive Ni is in the form of free NiO [10-11, 23, 26-27, 29-32, 41, 43, 53]. This can be right when the reactivity of $NiAl_2O_4$ is low, as seems to be the case for particles prepared by freeze granulation, mechanical mixing or spray dried methods. Nevertheless, for the impregnated particles used in this work, both NiO and $NiAl_2O_4$ are

present in the oxygen carrier and both of them react with the fuel. Therefore, both compounds must be considered in design calculations To calculate the average reactivity in this case, it was assumed that a fraction of Ni is entering to the fuel reactor as NiO and another fraction as $NiAl_2O_4$. The average reactivity can be obtained as

$$\left[\overline{\frac{dX_s}{dt}}\right] = R_m = f_{NiO}\Delta X_s\left[\overline{\frac{dX_{NiO}}{dt}}\right] + (1 - f_{NiO}\Delta X_s)\left[\overline{\frac{dX_{NiAl_2O_4}}{dt}}\right] \quad (14)$$

where f_{NiO} is the fraction of the reduced nickel that it is oxidized into free NiO in the AR. From the results obtained in this work, f_{NiO} for Ni18-αAl oxygen carrier is 0.8. The product $f_{NiO}\cdot\Delta X_s$ is the fraction of NiO in the oxygen carrier after oxidation whereas 1-$f_{NiO}\cdot\Delta X_s$ is the fraction of $NiAl_2O_4$.

The conversion curves from the TGA in Figure 7 can be divided into two sections: the fast reduction of free NiO initially and, after that, a stage with lower reactivity corresponding to $NiAl_2O_4$ reaction with the fuel. The reduction of NiO was considered to be separated from this of $NiAl_2O_4$ and each reaction period was transformed to have a conversion between 0 and 1, corresponding to the evolution of the reaction of NiO and $NiAl_2O_4$ with time. Figure 10 shows the conversion curves for NiO and $NiAl_2O_4$. In both cases the reactivity curves are overlapped, indicating that the reactivity of NiO and $NiAl_2O_4$ does not depend on the fraction of each phase in the oxygen carrier. The average reactivity, $\overline{\frac{dX_s}{dt}}$, for both nickel compounds was obtained as the slope of the curve at X_s=0. The values were 0.15 and 4.2 x 10^{-3} s^{-1} for NiO and $NiAl_2O_4$, respectively. NiO average reactivity was higher than for $NiAl_2O_4$ as expected.

Figure 11 shows the average reactivity of Ni18-αAl oxygen carrier for the reduction reaction calculated using Equation 14 as a function of the variation of solid conversion in the fuel reactor. The average reactivity increased with ΔX_s due to the increase in the

amount of the highly reactive NiO in the oxygen carrier with an increasing solid conversion. When only NiO is initially present in the oxygen carrier, and after its reduction, it is reoxidized completely to NiO ($f_{NiO} = 1$), the average reactivity is the one that corresponds to NiO. This NiO average reactivity has been also depicted as a reference in Figure 11 in the form of a straight line. If f_{NiO} was 1 instead 0.8, i.e. all reduced Ni was oxidized to NiO, the average reactivity of NiO-$NiAl_2O_4$ at $\Delta X_s = 1$ would coincide with NiO reactivity. As $f_{NiO} = 0.8$, a lower value was obtained.

In a CLC plant, each particle of oxygen carrier has a different residence time in the fuel reactor so this fact must be considered in the design. Taking into account that the solids in the fuel reactor are in perfect mixing and a shrinking core model for the gas-solid reaction, the average reactivities for NiO and $NiAl_2O_4$ can be obtained similarly to the method described by Abad et al [11]

$$\left[\overline{\frac{dX_{NiO}}{dt}}\right] = \frac{3}{\tau_{NiO}}\left[1 - X_{in,FR}^{2/3} e^{-\left[\tau_{NiO}(1-X_{in,FR}^{1/3})\frac{R_m}{\Delta X_s}\right]}\right] - \frac{6\Delta X_s}{\tau_{NiO}^{2} R_m}\left[1 - X_{in,FR}^{1/3} e^{-\left[\tau_{NiO}(1-X_{in,FR}^{1/3})\frac{R_m}{\Delta X_s}\right]}\right] + \frac{6\Delta X_s^{2}}{\tau_{NiO}^{3} R_m}\left[1 - e^{-\left[\tau_{NiO}(1-X_{in,FR}^{1/3})\frac{R_m}{\Delta X_s}\right]}\right] \quad (15)$$

$$\left[\overline{\frac{dX_{NiAl_2O_4}}{dt}}\right] = \frac{3}{\tau_{NiAl_2O_4}}\left[1 - X_{in,FR}^{2/3} e^{-\left[\tau_{NiAl_2O_4}(1-X_{in,FR}^{1/3})\frac{R_m}{\Delta X_s}\right]}\right] - \frac{6\Delta X_s}{\tau_{NiAl_2O_4}^{2} R_m}\left[1 - X_{in,FR}^{1/3} e^{-\left[\tau_{NiAl_2O_4}(1-X_{in,FR}^{1/3})\frac{R_m}{\Delta X_s}\right]}\right] + \frac{6\Delta X_s^{2}}{\tau_{NiAl_2O_4}^{3} R_m}\left[1 - e^{-\left[\tau_{NiAl_2O_4}(1-X_{in,FR}^{1/3})\frac{R_m}{\Delta X_s}\right]}\right] \quad (16)$$

To obtain these equations, it was considered that the residence time distributions (RTD) of both NiO and $NiAl_2O_4$ in the fuel reactor were the same. Indeed, NiO and $NiAl_2O_4$ are mixed in the same particle. R_m is defined by Equation 14. $X_{in,\ FR}$ is the solid

conversion at the inlet of the fuel reactor and ΔX_s is the variation of solid conversion in the reactor.

The values for τ_{NiO} and $\tau_{NiAl2O4}$ should be obtained at an average gas concentration in the bed, after the determination of the kinetic parameters using shrinking core model. Equation 17 shows the relation between the values of τ_i and $\frac{dX_s}{dt}$ at $X_s = 0$ as

$$\tau_i = \frac{3}{\left(\frac{dX_s}{dt}\right)} \quad (17)$$

τ_{NiO} and $\tau_{NiAl_2O_4}$ were 20 and 718 s, respectively.

Figure 11 also shows the average reactivity when the residence time distribution (RTD) in the fuel reactor is considered with only NiO in the oxygen carrier, and this is oxidized again to NiO after its reaction with the fuel. Initially, when $\Delta X_s \rightarrow 0$, the average reactivity coincides with NiO reactivity without perfect mixing of the oxygen carrier in the FR (0.15 s^{-1}). However, the average reactivity decreases with an increasing ΔX_s, because the residence time in FR to achieve full conversion of the fuel should be higher. The reactivity curve when NiO and $NiAl_2O_4$ are present in the oxygen carrier shows a maximum due to the combined effect of the variation of reactivity with the fraction of NiO and $NiAl_2O_4$ and RTD as a function of ΔX_s. When ΔX_s was low, the increase in the relative amount of NiO had a dominant effect and the average reactivity increased as ΔX_s increased. When ΔX_s increased, with more NiO in the solid, the importance of the residence time became more significant, and average reactivity decreased.

Additionally, it can be seen in Figure 11 that the reactivity of the Ni18-αAl oxygen carrier was about one order of magnitude lower than if all Ni was as free NiO, indicating the negative effect of the formation of $NiAl_2O_4$. The decrease in the reactivity will also affect the solid inventory needed in the system, which should be about 10

times higher than the expected if the formation of $NiAl_2O_4$ was avoided. Nevertheless, and despite the presence of nickel aluminate, the use of the Ni18-αAl oxygen carrier has been successfully demonstrated in previous works [44, 47-49] reaching high combustion efficiencies without carbon formation or agglomeration problems in a CLC continuous pilot plant.

5. Conclusions

The reactivity of a Ni-based oxygen carrier prepared by hot incipient wetness impregnation method and containing 18 wt% NiO was analyzed by means of pulse experiments in a batch fluidized bed reactor and TGA.

With the pulse experiments, CH_4 conversion, secondary reactions and $NiO/NiAl_2O_4$ distribution in the Ni18-αAl oxygen carrier were analyzed. Together with the direct reaction of CH_4 with the oxygen carrier, it was found that CH_4 steam reforming was a significant reaction, catalyzed by reduced Ni in the oxygen carrier and with CO and H_2 as intermediate products. Carbon formation did not take place in the system.

Different reactivities of the oxygen carrier were observed depending on the conversion reached during the reduction stage. These differences were attributed to different free NiO and $NiAl_2O_4$ contents in the samples. From the experiments in the batch fluidized bed reactor and additional test in TGA, it was determined that, regardless ΔX_s, 80% of Ni reduced in the FR was oxidized to free NiO while the remaining Ni was oxidized into $NiAl_2O_4$.

The presence of $NiAl_2O_4$ affects the reactivity of the oxygen carrier with the fuel, so it needs to be considered in the design of a CLC system. The lower reactivity of $NiAl_2O_4$ with respect to free NiO causes a decrease in the average reactivity in the fuel reactor, but, despite this, high conversion of fuel gas can be reached in a CLC system. The

average reactivity of the oxygen carrier vs. ΔX_s curve shows a maximum value due to the combined effect on the reactivity of the residence time in the reactor and the relative amount of NiO.

Notation

d = stoichiometric factor in the combustion reaction of the fuel with oxygen (mol O_2 per mol of fuel)

ΔH_c^o = standard heat of combustion of the fuel gas (kJ mol^{-1})

f_{NiO} = fraction of the reduced Ni which is oxydized into NiO in the AR

M_O = molecular weight of oxygen (16 g mol^{-1})

m = actual mass of the oxygen carrier (kg)

m_{ox} = mass of the fully oxidized oxygen carrier (kg)

m_{red} = mass of the fully reduced oxygen carrier (kg)

m_{OC} = solid inventory, as fully oxidized oxygen carrier, in the FR (kg OC MW_f^{-1})

$\dot{m}_{OC}$ = circulation rate of the fully oxidized oxygen carrier (kg OC $s^{-1}MW_f^{-1}$)

n_i = number of moles of gas i measured during the reduction time of a redox cycle (mol)

n_O = number of oxygen moles available for the reduction reaction in the oxygen carrier (mol)

$P_{i,\,out}$ = partial pressure of gas i in the outlet stream of the batch fluidized bed reactor

R_m = Average reactivity (s^{-1})

R_{OC} = Oxygen transport capacity of the oxygen carrier (kg O kg OC^{-1})

$X_{in,\,FR}$ = solid conversion at the inlet of the FR

X_s = solid conversion in reduction reaction

ΔX_g = variation of the gas conversion

ΔX_s = variation of the solid conversion

Greek letters

γ_i = normalized concentration of gas i

τ_i = time for complete solid conversion for the reaction i (s)

Acknowledgements

This research was conducted with financial support from the Spanish Ministry of Science and Technology (Project No. CTQ2007-64400). C. Dueso thanks MICIN for a FPI fellowship. C. Dueso thanks Erik Jerndal his valuable help with the experimental work during her stay at Chalmers University of Technology, Göteborg, Sweden.

References

[1] IPCC, 2005: IPCC Special Report on Carbon Dioxide Capture and Storage. Prepared by Working Group III of the Intergovernmental Panel on Climate Change Eds. Metz B, Davidson O, de Coninck HC, Loos M, and Meyer LA. Cambridge University Press, Cambridge, United Kingdom and New York, NY, USA. 2005.

[2] IPPC, 2007: Climate change 2007: The Physical Science Basis. Working Group I Contribution to the Fourth Assessment Report of The International Panel on Climate Change. Eds. Solomon S, Qin D, Manning M, Marquis M, Averyt K, Tignor MMB, Miller HL. Cambridge University Press, Cambridge, United Kingdom and New York, NY, USA 2007.

[3] Richter H, Knoche K. Reversibility of combustion process. In: Gaggioli RA, editor. Second law analysis of processes. ACS Symposium Series 235, Washington, DC, 1983. p. 71-85.

[4] Wolf J, Anheden M, Yan J. Comparison of nickel- and iron-based oxygen carriers in chemical looping combustion for CO_2 capture in power generation. Fuel 2005; 84: 993–1006.

[5] Kvamsdala H M, Jordala K, Bolland O. A quantitative comparison of gas turbine cycles with CO_2 capture. Energy 2007; 32: 10–24.

[6] Ishida M, Sheng D, Akehata T. Evaluation of a chemical-looping combustion power-generation system by graphic exergy analysis. Energy 1987; 12: 147-54.

[7] Anheden M, Svedberg G. Exergy analysis of chemical-looping combustion systems. Energy Convers Management 1998; 39: 1967-80.

[8] Ishida M, Jin H. A novel chemical-looping combustor without NO_x formation. Ind Eng Chem Res 1996; 35(7): 2469-72.

[9] Lyngfelt A, Leckner B, Mattisson T. A fluidized-bed combustion process with inherent CO_2 separation; application of chemical-looping combustion. Chem Eng Sci 2001; 56: 3101-13.

[10] Adánez J, de Diego L F, García-Labiano F, Gayán P, Abad A, Palacios J M. Selection of oxygen carriers for chemical-looping combustion. Energy Fuels 2004; 18(2): 371-77.

[11] Abad A, Adánez J, García-Labiano F, de Diego L F, Gayán P, Celaya J. Mapping of the range of operational conditions for Cu-, Fe-, and Ni-based oxygen carriers in chemical-looping combustion. Chem Eng Sci 2007; 62(1-2): 533-49.

[12] Hossain, M M, de Lasa H I. Chemical-looping combustion (CLC) for inherent CO_2 separations-A review. Chem Eng Science 2008; 63: 4433-51.

[13] Adánez J, García-Labiano F, de Diego L F, Gayán P, Celaya J, Abad A. Nickel−copper oxygen carriers to reach zero CO and H_2 emissions in chemical-looping combustion. Ind Eng Chem Res 2006; 45 (8): 2617-25.

[14] Abad A, Mattisson T, Lyngfelt A, Johansson M. The use of iron oxide as oxygen carrier in a chemical-looping reactor. Fuel 2007; 86: 1021–35.

[15] Corbella B, Palacios J M. Titania-supported iron oxide as oxygen carrier for chemical-looping combustion of methane. Fuel 2007; 86: 113–22.

[16] García-Labiano F, Adánez J, de Diego L F, Gayán P, Abad A. Effect of pressure on the behavior of copper-, iron-, and nickel-based oxygen carriers for chemical-looping combustion. Energy Fuels 2006; 20: 26-33.

[17] Ishida M, Takeshita K, Suzuki K, Ohba T. Application of Fe_2O_3−Al_2O_3 composite particles as solid looping material of the chemical-loop combustor. Energy Fuels 2005; 19 (6): 2514-18.

[18] Johansson M, Mattisson T, Lyngfelt A. Investigation of Fe_2O_3 with $MgAl_2O_4$ for Chemical-Looping Combustion. Ind Eng Chem Res 2004; 43 (22): 6978-87.

[19] de Diego L F, Gayán P, García-Labiano F, Celaya J, Abad A, Adánez J. Impregnated CuO/Al_2O_3 oxygen carriers for chemical-looping combustion: avoiding fluidized bed agglomeration. Energy Fuels 2005; 19: 1850-56.

[20] García-Labiano F, de Diego L F, Adánez J, Abad A, Gayán P. Reduction and oxidation kinetics of a copper-based oxygen carrier prepared by impregnation for chemical-looping combustion. Ind Eng Chem Res 2004; 43: 8168-77.

[21] Hoteit A, Chandel M, Delebarre A. Nickel- and copper-based oxygen carriers for chemical looping combustion. Chem Eng Technol 2009; 32: 443-49.

[22] Abad A, Mattisson T, Lyngfelt A, Rydén M. Chemical-looping combustion in a 300 W continuously operating reactor system using a manganese-based oxygen carrier. Fuel 2006; 85: 1174–85.

[23] Johansson M, Mattisson T, Lyngfelt A. Comparison of oxygen carriers for chemical-looping combustion. Thermal Science 2006; 10(3): 93-107.

[24] Johansson M, Mattisson T, Lyngfelt A. Investigation of Mn_3O_4 with stabilized ZrO_2 for chemical-looping combustion. Chem Eng Res and Design 2006; 84(A9): 807–18.

[25] Mattisson T, Järdnäs A, Lyngfelt A. Reactivity of some metal oxides supported on alumina with alternating methane and oxygen – Application for chemical-looping combustion. Energy Fuels 2003; 17: 643-51.

[26] Mattisson T, Johansson M, Lyngfelt A. The use of NiO as an oxygen carrier in chemical-looping combustion. Fuel 2006; 85: 736-47.

[27] Ishida M, Yamamoto M, Ohba T. Experimental results of chemical-looping combustion with $NiO/NiAl_2O_4$ particle circulation at 1200 ºC. Energy Conv Management 2002; 43: 1469-78.

[28] Cho P, Mattisson T, Lyngfelt A. Comparison of iron, nickel, copper and manganese-based oxygen carriers for chemical-looping combustion. Fuel 2004; 83: 1215-25.

[29] Jin H, Okamoto T, Ishida M. Development of a novel chemical-looping combustion: synthesis of a solid looping material of $NiO/NiAl_2O_4$. Ind Eng Chem Res 1999; 38: 126-32.

[30] Sedor K E, Hossain M M, de Lasa H I. Reactivity and stability of Ni/Al_2O_3 oxygen carrier for chemical-looping combustion (CLC). Chem Eng Science 2008, 63: 2994-3007.

[31] Jerndal E, Mattisson T, Lyngfelt A. Investigation of different $NiO/NiAl_2O_4$ particles as oxygen carriers for chemical-looping combustion. Energy Fuels 2009; 23(2): 665-76.

[32] Zafar Q, Mattisson T, Gevert B. Redox investigation of some oxides of transition-state metals Ni, Cu, Fe, and Mn supported on SiO_2 and $MgAl_2O_4$. Energy Fuels 2006; 20: 34-44.

[33] Villa R, Cristiani C, Groppi G, Lietti L, Forzatti P, Cornaro U, Rossini S. Ni based mixed oxide materials for CH_4 oxidation under redox cycle conditions. J. of Molecular Catalysis A: Chemical 2003; 204-205: 637-46.

[34] Cheng Z, Wu Q, Li J, Zhu Q. Effects of promoters and preparation procedures on reforming of methane with carbon dioxide over Ni/Al_2O_3 catalyst. Catalysis Today 1996; 30: 147-55.

[35] HSC Chemistry 6.1® 6.1. 2008. Chemical Reaction and Equilibrium Software with Thermochemical Database and Simulation Module. Oututec Research Oy.

[36] Cho P, Mattisson T, Lyngfelt A. Carbon formation on nickel and iron oxide-containing oxygen carriers for chemical-looping combustion. Ind Eng Chem Res 2005; 44 (4): 668-76.

[37] Ryu H-J, Bae D-H, Jin G-T. Effects on reduction temperature of oxygen carrier particles on a fixed bed chemical-looping combustion. Korean Journal of Chemical Engineering 2003; 20: 960–66.

[38] Gayán P, de Diego, L F, García-Labiano F, Adánez J, Abad A, Dueso C. Effect of support on reactivity and selectivity of Ni-based oxygen carriers for chemical-looping combustion. Fuel 2008; 87: 2641-50.

[39] Rydén M, Lyngfelt A. Using steam reforming to produce hydrogen with carbon dioxide capture by chemical-looping combustion. International Journal of Hydrogen Energy 2006; 31: 1271-83.

[40] Rydén M, Lyngfelt A, Mattisson T. Synthesis gas generation by chemical looping reforming in a continuously operating laboratory reactor. Fuel 2006; 85: 1631-41.

[41] Shulman A, Linderholm C, Mattisson T, Lyngfelt A. High reactivity and mechanical durability of $NiO/NiAl_2O_4$ and $NiO/NiAl_2O_4/MgAl_2O_4$ oxygen carrier

particles used for over 1000 hours in a 10 kW CLC reactor. Ind Eng Chem Res 2009, 48(15): 7400-05.

[42] Bolt P H, Habraken F H P M, Geus J W. Formation of nickel, cobalt, copper and iron aluminates from α- and γ-alumina-supported oxides: a comparative study. Journal of solid state chemistry 1998; 135: 59-69.

[43] Gayán P, Dueso C, Abad A, Adánez J, de Diego L F, García-Labiano F. NiO/Al_2O_3 oxygen carriers for chemical-looping combustion prepared by impregnation and deposition-precipitation methods. Fuel 2009; 88: 1016-23.

[44] Adánez J, Dueso C, de Diego L F, García-Labiano F, Gayán P, Abad A. Methane combustion in a 500 Wth Chemical-Looping Combustion system using an impregnated Ni-based oxygen carrier. Energy Fuels 2009; 23(1): 130-42.

[45] Johansson M, Mattisson T, Lyngfelt A, Abad A. Using continuous and pulse experiments to compare two promising nickel-based oxygen carriers for use in chemical-looping technologies. Fuel 2008; 87: 988-1001.

[46] Levenspiel O. Chemical Reaction Engineering. John Wiley & Sons Inc. 1999.

[47] García-Labiano F, de Diego L F, Gayán P, Adánez J, Abad A, Dueso C. Effect of fuel gas composition in Chemical-Looping Combustion with Ni-based oxygen carriers. 1. Fate of sulfur. Ind Eng Chem Res 2009: 48(5): 2499-2508.

[48] Adánez J, Dueso C, de Diego L F, García-Labiano F, Gayán P, Abad A. Effect of fuel gas composition in Chemical-Looping Combustion with Ni-based oxygen carriers. 2. Fate of light hydrocarbons. Ind Eng Chem Res 2009; 48(5): 2509-18.

[49] Dueso C, García-Labiano F, Adánez J, de Diego L F, Gayán P, Abad A. Syngas combustion in a chemical-looping combustion system using an impregnated Ni-based oxygen carrier. Fuel 2009; 88: 2357-64.

[50] Li C, Chen Y-W. Temperature-programmed-reduction studies of nickel oxide/alumina catalysts: effects of the preparation method. Thermochimica Acta 1995; 256: 457-65.

[51] Gil A, Díaz A, Gandía L M, Montes M. Influence of the preparation method and the nature of the support on the stability of nickel catalysts. Applied Catalysis A: General 1994; 109: 167-79.

[52] Huang Y-J, Schwarz J A. Effect of catalyst preparation on catalytic activity. VII. The chemical structures on nickel/alumina catalysts: their impact on the formation of metal-support interactions. Applied Catalysis 1988; 37: 229-45.

[53] Abad A, García-Labiano F, de Diego L F, Gayán P, Adánez J. Reduction kinetics of Cu-, Ni- and Fe-based oxygen carriers using syngas ($CO+H_2$) for chemical-looping combustion. Energy Fuels 2007; 21: 1843-53.

Table 1. Properties of the oxygen carrier Ni18-αAl as prepared (fresh) and used for 100 hours in a 500 W_{th} continuous pilot plant with CH_4 as fuel.

	fresh	used
NiO content (wt%)	18	18
Oxygen transport capacity, R_{OC}	0.0386	0.0386
Particle size (μm)	0.1-0.3	0.1-0.3
Porosity (%)	0.4	0.42
Solid density (kg m^{-3})	4290	4250
Specific surface area BET (m^2 g^{-1})	7.0	6.8
Crushing strength (N)	4.1	3.7
XRD phases	α-Al_2O_3, NiO, $NiAl_2O_4$	α-Al_2O_3, NiO, $NiAl_2O_4$
% Ni as NiO (%)	65	24

Table 2. Reaction times in the reduction stage used during the 10-redox-cycle experiments in the TGA.

Test	No. cycles	Reduction time (s)	Oxidation time (s)	X_s
A	10	6	180	28
B	10	12	180	32
C	10	20	180	35
D	10	30	180	52
E	10	60	180	68
F	4	Time to full conversion	180	96

Figure 1. Solid conversion and gas concentrations during the reduction period of a pulse experiment with 12 pulses of 4 s (dry basis).

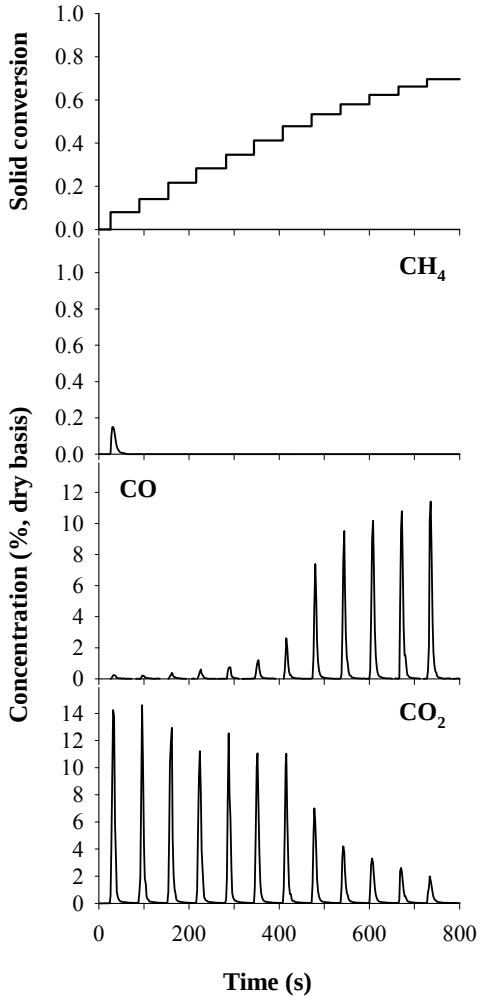

Figure 2. Concentration profiles from a redox cycle with 10 CH_4 pulses of 4 s during the reduction period. Pulse 1 (——), 4 (·····), 6 (- - - -), 8 (- · - · -) and 10 (– – –).

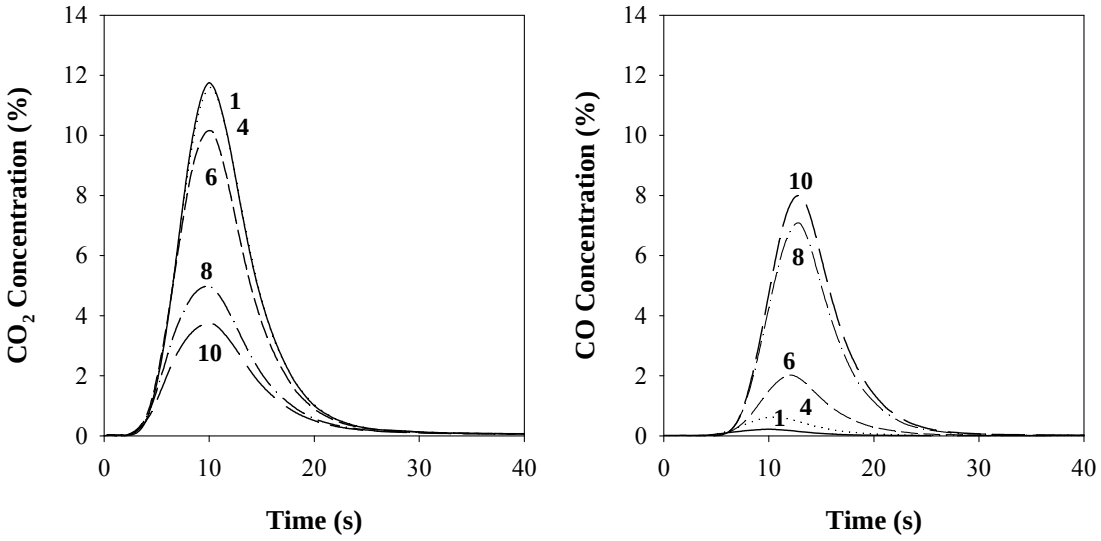

Figure 3. CO_2 and CO normalized concentrations in (a) 4 pulse and (b) 10 pulse experiments during cycles 1(——), 2 (.....), 4 (- - - -), 6 (– – –), 8 (– · – ·) and 10 (– · –) as a function of the solid conversion reached.

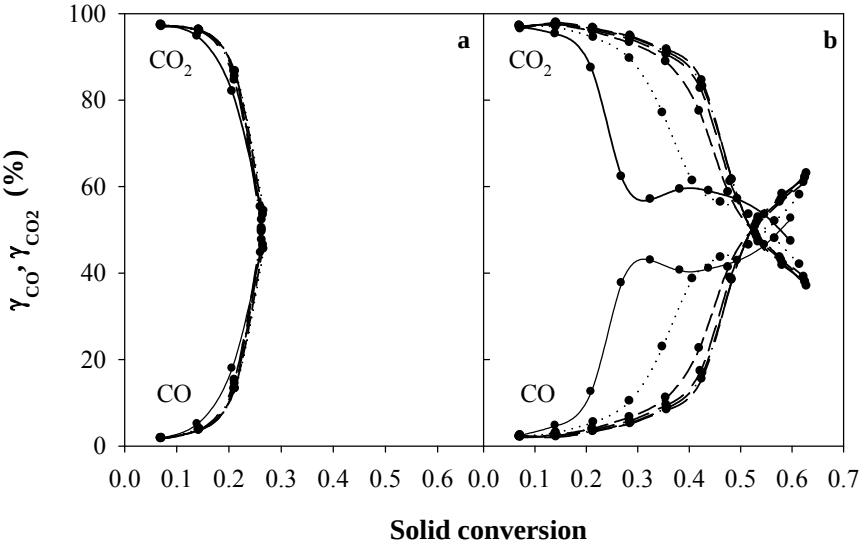

Figure 4. Solid conversion to reach a CO_2 normalized concentration in the outlet gases of the batch fluidized bed reactor of 90 % with the number of cycles for experiments with 2 (●), 4 (▲), 6 (■), 8 (◆), 10 (○) and 12 (□) pulses during the reduction time.

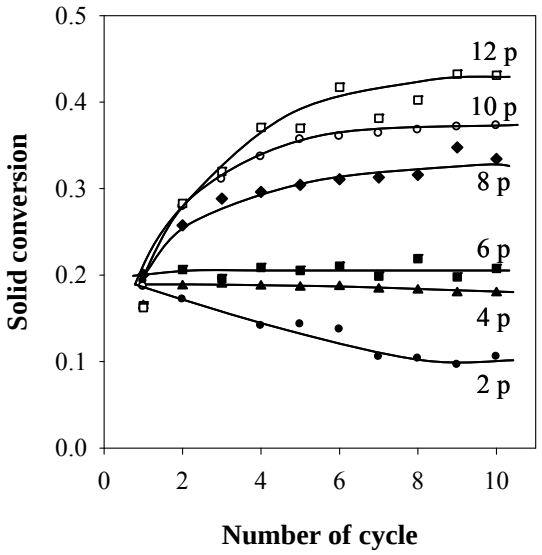

Figure 5. Solid conversion vs. time for the reference cycle after experiments with 2(——), 4 (- - - -), 6 (.....), 8 (– – –), 10 (– · – · –) and 12 (– · · – · · –) pulses during the reduction period and reference cycle (–●–) with the initial sample.

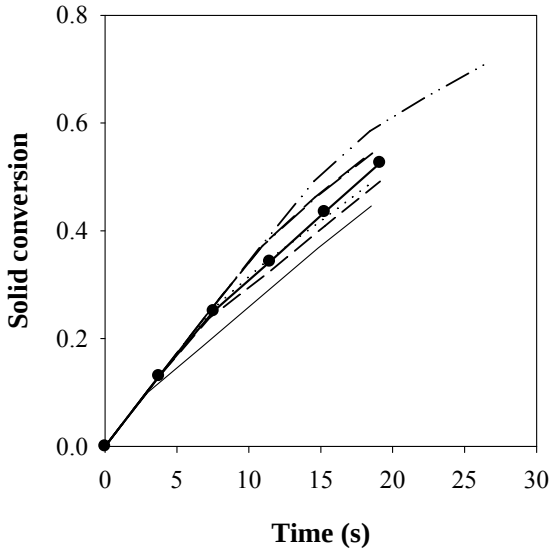

Figure 6. Fraction of Ni as free NiO in the oxygen carrier as a function of the solid conversion reached during the pulse experiments. ● corresponds to the NiO fraction of the initial sample with the conversion reached in the tests in the 500 W_{th} pilot plant. – – - represents the amount of free NiO in the oxygen carrier when $NiAl_2O_4$ is not present in the sample.

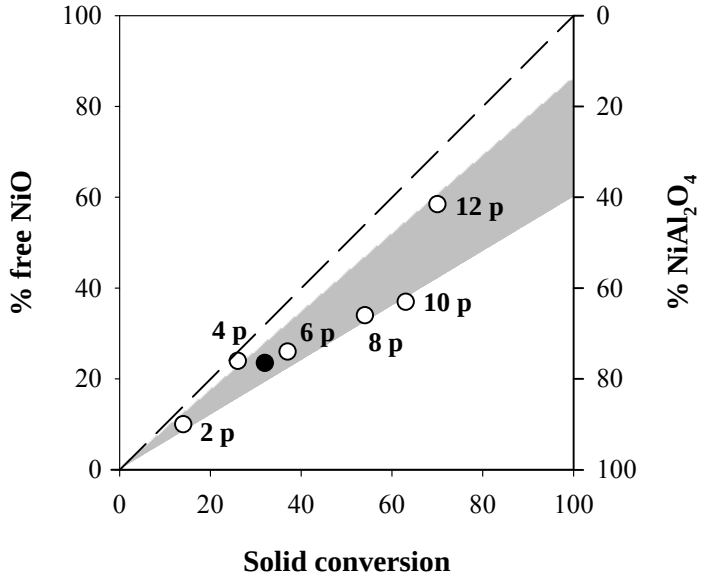

Figure 7. TGA reactivity data for the reduction during the reference tests after experiments A (_..._), B (_._._), C (.....), D (_ _ _), E (- - - -) and F (____) from Table 2. T = 1223 K. 5 vol.% H_2; 21% O_2.

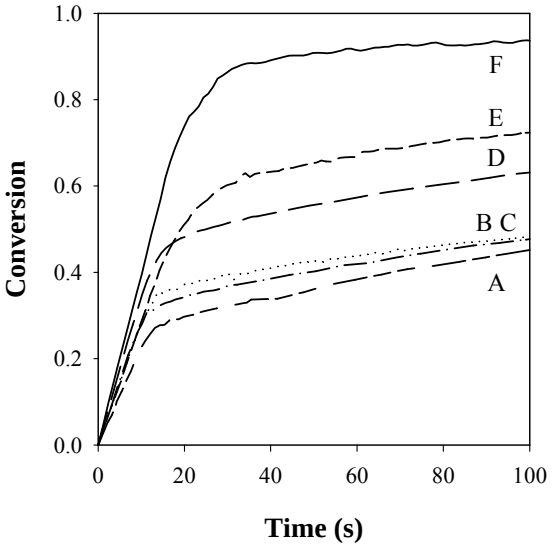

Figure 8. (a) TPR of the samples after TGA experiments in Table 2 (b) Solid conversion during TPR after TGA experiments from Table 2. A (_ . . _), B (_ . _), C (.....), D (- - - -), E (_ _ _) and F (____).

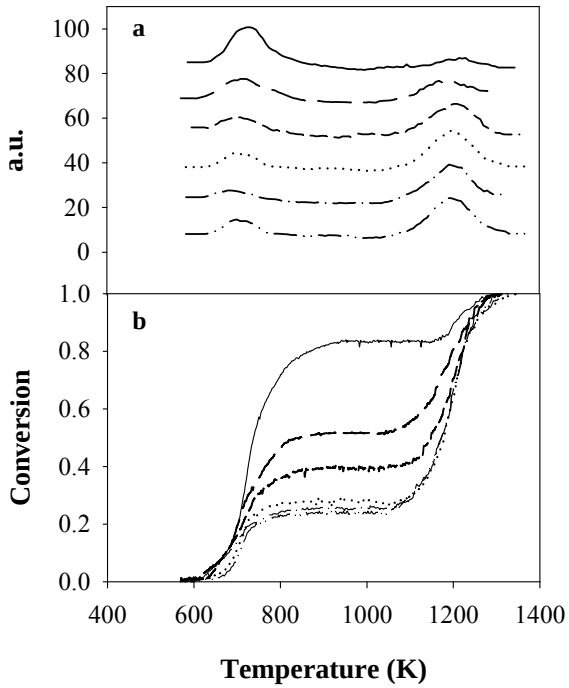

Figure 9. Fraction of Ni as NiO in the oxygen carrier as a function of the solid conversion reached in the TGA experiments.

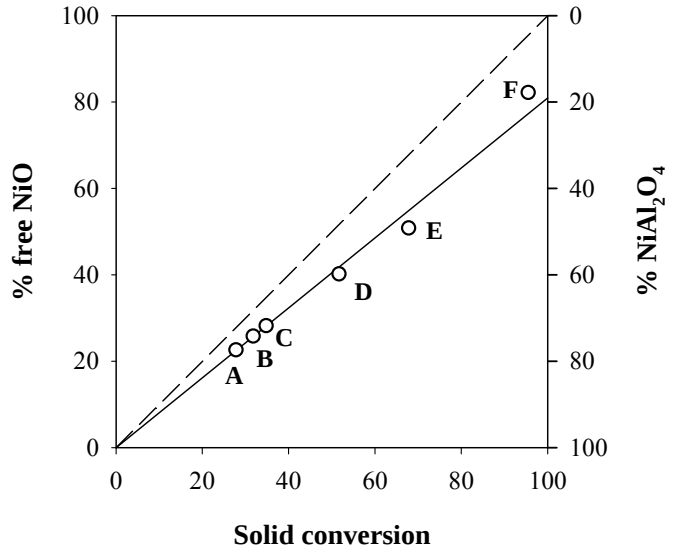

Figure 10. TGA reactivity for NiO and $NiAl_2O_4$ for experiments from Table 2. A (_ · _), B (_ _), C (.....), D (- - - -), E (_ _ _) and F (____).5 vol.% H_2; T = 1223 K.

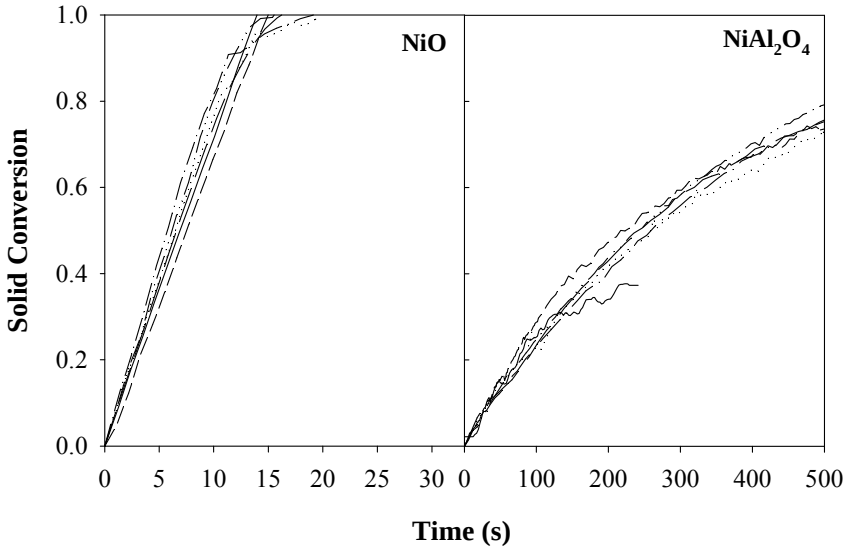

Figure 11. Average reactivity of the Ni18-αAl oxygen carrier when only NiO or both NiO and $NiAl_2O_4$ present in the solid react with the fuel. (_ · _) Reactivity of NiO at X_s = 0; (_ _ _) Reactivity of NiO + $NiAl_2O_4$ at X_s = 0; (_ · · _) Reactivity of NiO considering the RTD of the solids; (____) Reactivity of NiO + $NiAl_2O_4$ considering the RTD of the solids.